metals

MDPI

Article

Influence of the Geometrical Aspect Ratio on the Magneto-Structural Properties of Co₂MnSi Microwires

Asma Wederni [1,2,3,*] , Mohamed Salaheldeen [1,2,3,4,*] , Mihail Ipatov [1,2], Valentina Zhukova [1,2,3] and Arcady Zhukov [1,2,3,5]

1 Department of Polymers and Advanced Materials, Faculty of Chemistry, University of the Basque Country, UPV/EHU, 20018 San Sebastián, Spain; mihail.ipatov@ehu.eus (M.I.); valentina.zhukova@ehu.eus (V.Z.); arkadi.joukov@ehu.eus (A.Z.)
2 Department of Applied Physics I, EIG, University of the Basque Country, UPV/EHU, 20018 San Sebastián, Spain
3 EHU Quantum Center, University of the Basque Country, UPV/EHU, 20018 San Sebastián, Spain
4 Physics Department, Faculty of Science, Sohag University, Sohag 82524, Egypt
5 IKERBASQUE, Basque Foundation for Science, 48011 Bilbao, Spain
* Correspondence: asma.wederni@ehu.eus (A.W.); mohamed.salaheldeenmohamed@ehu.eus (M.S.)

Abstract: This present study illustrates the strong effect of geometrical parameters on the magneto-structural properties of Co₂MnSi glass-coated microwires prepared using the Taylor–Ulitovsky method. Thus, there are three samples with different geometrical aspect ratios (ρ). The XRD analysis shows a significant change by modifying the aspect ratio; for $\rho = 0.42$, the main peak with miller indices (220) is recognized as an A2-type disordered cubic structure. For the sample with $\rho = 0.46$, mixed L2₁ and B2 cubic structures are observed. Meanwhile, in the sample with a low aspect ratio, $\rho = 0.30$, the perfect L2₁ ordered cubic structure is attained. Magnetic characterization has been carried out at a wide range of temperatures and magnetic fields. A significant increase in coercivity and normalized reduced remanence by decreasing the aspect ratio is detected. The change in the magnetic properties is attributed to the modification in the microstructure, which is induced during the fabrication process. Such a dependence on the microstructure and magnetic properties on the ρ-ratio can be associated either with the internal stress distribution and magnitude or with different quenching rates of microwires with different aspect ratios. The current findings demonstrate the tunability of the microstructure and magnetic properties of Co₂MnSi-glass-coated microwires simply via a small modification in the geometric properties during the manufacturing process and without excreting any additional post-processing. The variation in the geometric parameters of Co₂MnSi glass-coated microwires allows us to tune the magnetic properties and structure, which is essentially advantageous for sensing device development.

Keywords: Heusler alloys; glass-coated microwires; L2₁ cubic structure; aspect ratio

1. Introduction

Investigations of innovative materials, particularly half-metals displaying ferromagnetism at a wide range of temperatures, have intensified due to the development of a new generation of spintronic devices [1]. Among the most extensively studied materials are the Heusler alloys, defined as magnetic intermetallic. The Heusler alloys present a vast family of ternary intermetallic compounds with a variety of magnetic phenomena. Several of such compounds are well known for their unique properties, such as high Curie temperature, half metallicity, and excellent tenability for metallic Heusler alloys are of particularly great interest due to the high spin-polarized current close to the Fermi level, which is predicted to increase the efficiency of spintronic devices. This can be exploited to enhance the efficiency of spin-injecting and information storage devices [2,3]. Depending on the nature of magnetic sub-lattices, a Heusler alloy is called either half-Heusler compounds or full-Heusler compounds [4,5].

Their generic formula is X_2YZ. In general, X and Y are d-group transition metal elements. X is usually a transition metal: 3d (Fe, Co, Ni, Cu, Zn), 4d (Ru, Rh, Pd, Ag, Cd), or 5d (Ir, Pt, Au). The position of Y is usually occupied by 3d (Ti, V, Cr, Mn), 4d (Y, Zr, Nb), 5d (Hf, Ta), or by lanthanides (Gd, Tb, Dy, Ho, Er, Tm, Yb, Lu) or actinides (U). Z is the p-group main element III-B (Al, Ga, In, Tl), IV-B (Si, Ge, Sn, Pb), or V-B (As, Sb, Bi) [6,7]. The parent phase may be stabilized using the covalent link created via the p-d orbital hybridization between p and d-group atoms. One of the most attractive materials for multiple-function applications is Co_2-based full/half-Heusler alloys with high Curie temperatures (Tc > 1100 K), high magnetic moments, distinct electronic structures, and low Gilbert damping constants (=0.004) [4,8]. Because of their distinctive electronic band structures, some Co_2-based full Heusler alloys also exhibit a significant anomalous Hall effect in addition to half-metallic ferromagnetism [9]. Accordingly, Co_2-based Heusler alloys have attracted the scientific community's attention and, therefore, have been widely explored experimentally. Over the past ten years, a theoretical and experimental study has been conducted to fully understand the crystalline structure [10,11]. Thus, two crystalline phases of Heusler alloys can be found: the high-symmetry austenite phase, which has the simplest structure as a cubic $L2_1$ (high-ordered phase) or B2 structure (disorder phase), and the less-symmetrical martensitic phase [6].

Using the appropriate manufacturing and synthesis procedures, alloys can acquire the ordered austenitic structure. In some cases, the $L2_1$ phase can be obtained by annealing the alloys at high temperatures for several hours, followed by a long cooling procedure to create a solid-state reaction [12]. In this instance, the formation of this phase is promoted via the homogenization of the chemical composition and the removal of impurities in the produced alloys [13,14]. Other synthesized techniques, like melt spinning or atomization, can also be used to obtain the $L2_1$ phase in Heusler alloys via rapid solidification. These procedures consist of quenching the molten alloy at a high cooling rate to eliminate the formation of other phases and promote the formation of the ordered one [14–17]. Otherwise, the formation of nanocrystalline powder alloys can lead to reaching the fully ordered $L2_1$ structure. Alternatively, mechanical alloying, consisting of milling a mixture of the constituent elements of the desired alloy in a ball milling for several hours or even days, can be used. Hereafter, the obtained powders can be consolidated into bulk materials by hot pressing or sintering [18]. It should be noted that the composition of the alloy and the processing techniques employed have a significant impact on the attainment of the $L2_1$ structure [15]. Depending on the material's desired qualities and intended applications, different processing conditions may be suitable.

Co_2Mn-based alloys with an $L2_1$ structure exhibit a ferromagnetic ordering, which makes them attractive for various magnetic applications [5,19]. In addition, this ordered structure is suitable for high-temperature applications [20]. Moreover, to describe the mechanical stability of alloys exhibiting an $L2_1$-ordered structure, the stability of some elastic constants against external forces was examined. When analyzing the elastic constants and other related mechanical properties, excellent mechanical properties, such as high strength, good ductility, and high fracture toughness, were observed [21]. Such properties are suitable for thermoelectric applications and the development of devices based on spintronics.

Recently, the Taylor–Ulitovsky technique involving rapid melt quenching has been successfully used for the fabrication of thin glass-coated magnetic microwires from Heusler alloys [22–25]. The Taylor–Ulitovsky process allows the preparation of a substantial amount (up to several km) of metallic microwires covered by glass coating from a few grams of master alloy within a few minutes [2,22,26,27]. As discussed elsewhere, such a fabrication technique provides a favorable surface-to-volume ratio, tunable diameter, d, of the metallic nucleus, and glass-coating thickness. Additionally, the internal stress magnitude is tunable by the ratio, ρ, between the metallic nucleus diameter, d, and total diameter, D [22]. The preferable axial origin of such internal stresses substantially affects the magnetic anisotropy and, particularly, the easy magnetization axis of glass-coated microwires [26,28]. Moreover,

the ability to fabricate glass-coated microwires with various structures (such as amorphous, nanocrystalline, and granular) offers a special advantage for researching the impact of various microstructures on the physical properties of the same material [27,28].

This current study is an extension of our previous investigations on the magneto-structural properties of Co_2Mn-based glass-coated microwires [19,29–33]. The main objective of this present study is to illustrate the influence of the aspect ratio change on the magneto-structural behavior of the well-known Co_2MnSi alloys for multifunctional applications.

2. Materials and Methods

The preparation of Co_2MnSi glass-coated microwires involves two essential steps. First of all, the melting process begins by melting the high purity (Co (99.99%), Mn (99.9%), and Si (99.9%)) elements in an arc melting furnace. The alloy components were weighed according to the desired composition and placed in a water-cooled copper mold. Manganese was supplemented with an extra two weight percent to compensate for the losses that can be caused by its evaporation during the production process. The melting procedure was repeated five times to obtain highly homogeneous alloy with a uniform microstructure [16,29,30]. At this stage, the Co_2MnSi alloy ingot was prepared, permitting us to proceed with the manufacturing of Co_2MnSi glass-coated microwires using the Taylor–Ulitovsky, technique [22,24,28–30]. Afterward, the obtained metal ingot (normally a few grams) is melted again inside a Pyrex glass tube by a high-frequency inductor (normally 350–500 kHz). A capillary is then formed from the softened glass, which is captured by a rotating receiving coil [22,26,27] Subsequently, a microwire with a metallic nucleus completely coated in a continuous, thin, and flexible glass covering is formed as the molten metallic alloy fills the glass capillary. In this fabrication process, a composite metallic microwire covered by insulating glass coating undergoes rapid solidification as it passes through a stream of coolant water [22,24]. Although the diameter of the metallic nucleus is limited by the master alloy droplet weight, the amount of glass employed in the process is balanced by the continuous passage of the glass tube through the inductor zone. One of the advantages of the Taylor–Ulitovsky procedure is that it allows the preparation of microwires with a very thin glass coating, typically a few micrometers in thickness. The metallic nucleus diameter, d, and glass-coating thickness can be adjusted by the speed at which the wire is drawn and by the glass tube feed rate. In this work, we have produced two types of Co_2MnSi glass-coated microwires with different geometrical parameters (the metallic nucleus and total diameters). The metallic nucleus, d, and the total microwire, D, diameters were tuned by adjusting the speed of wire drowning and pick-up bobbin rotation [22]. This manufacturing process is particularly advantageous for alloys containing manganese, as it protects against oxidation by the surrounding glass layer due to the rapid solidification [29]. The origins of mechanical internal stresses in glass-coated ferromagnetic microwires are attributed to several factors, such as the difference in the thermal expansion coefficients of metallic alloys solidifying inside the glass coating, the quenching stresses related to the rapid quenching of the metallic alloy, and the drawing stresses [22,26–36]. The internal stresses induced by the difference in the thermal expansion coefficients of the metallic alloy and the glass coating are the largest, being an order of magnitude higher than the other stresses [22,26,36,37]. The ratio of the metallic nucleus to the total diameter (d/D) can be used to estimate the first type of stress: stresses induced by the difference in the thermal expansion coefficients of the metallic alloy and the glass coating. It means that an increase in the d/D correlates with a decrease in the stress induced by the glass coating [22,26,33,36,37]. Henceforward, using an optical microscope, we can extract the diameters of microwires after their production, one with an aspect ratio of ρ = d/D = 0.42 and the other with ρ = d/D = 0.30. Therefore, in this work, two groups of Co_2MnSi glass-coated microwires with different d/D (9.6 μm/ 22.8 μm) and (7.1 μm/ 23.6 μm) were produced and investigated.

A scanning electron microscope connected to an energy-dispersive spectrometry (EDX) device was used to study the microstructure, morphology, and composition of the obtained

glass-coated microwires. In addition, their structural analysis was carried out using a BRUKER X-ray diffractometer (D8 Advance, Bruker AXS GmbH, Karlsruhe, Germany), performed using Cu Kα (λ = 1.54 Å) radiation. Magnetic properties of Co_2MnSi glass-coated microwires are carried out using a Physical Property Measurement System (PPMS) (Quantum Design Inc., San Diego, CA, USA). Measurements of the magnetization curves were performed parallel to the wire axis, where the easy magnetization direction is expected due to the shape magnetic anisotropy, and were carried out over a wide temperature range (5–300 K) and magnetic fields (50 Oe–1 kOe). To examine the potential magnetic phase transition or irreversibility, zero-field cooling (ZFC), field cooling (FC), and field heating (FH) protocols were used. The results are expressed as the normalized magnetization, M/M_{5K}, where M_{5K} is the magnetic moment obtained at 5 K.

3. Results

3.1. Microstructure Analysis

To investigate the aspect ratio effect in Co_2MnSi glass-coated microwires (GCMWs) produced using the Taylor–Ulitovsky process, two microwires with different d/D characteristics were selected. The first microwire shows the average metal core (d) and total (D) diameters of 7.1 and 23.6 µm, respectively (see Figure 1). The second microwire presents the average metal core (d) and total (D) diameters of 9.6 and 22.8 µm, respectively. We conducted an EDX/SEM study to determine the real chemical composition of the produced glass-coated microwires, and the output results are provided in Table 1. The actual chemical composition is determined by analyzing ten distinct locations. From such experiments, we determined that the average chemical composition of (GCMW-A) corresponds to $Co_{49.55}Mn_{25.1}Si_{25.02}$ and $Co_{51}Mn_{23.7}Si_{25.3}$ for (GCMW-B), which are close to the expected composition ($Co_{50}Mn_{25}Si_{25}$) and confirm the stoichiometric ratio (2:1:1), as listed in Table 1.
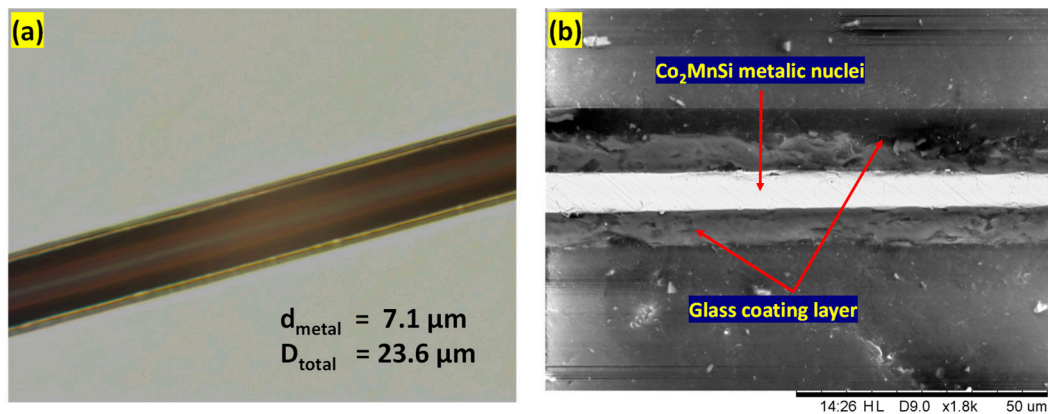

Figure 1. (**a**) Optical microscope and (**b**) SEM images of GCMWs-A illustrate the metallic nuclei of Co_2MnSi and coating layer.

Table 1. Chemical compositions and different aspect ratios of Co_2MnSi glass-coated microwires (GCMWs-A and GCMWs-B).

Sample	d (µm)	D (µm)	Aspect Ratio (ρ)	Chemical Composition
GCMWs-A	7.1 ± 0.1	23.6 ± 0.1	0.30 ± 0.01	$Co_{50}Mn_{25}Si_{25}$
GCMWs-B	9.6 ± 0.1	22.8 ± 0.1	0.42 ± 0.01	$Co_{50}Mn_{25}Si_{25}$
GCMWs**	10.2 ± 0.1	22.2 ± 0.1	0.46 ± 0.01	$Co_{51}Mn_{24}Si_{25}$

GCMWs**: Co_2MnSi glass-coated microwires with (ρ = 0.46) [29].

In addition, XRD structure analysis was conducted to explore the order state of Co_2MnSi-GCMWs and study the impact of the aspect ratio on the crystalline structure. The representative findings are illustrated in Figure 2. The (111) and (200) superlattice reflections are clearly observed at $2\Theta = 27.67^0$ and 32^0 positions in the XRD diffractogram for GCMW-A,

i.e., $\rho = 0.3$. As described in our previous publications [15,17,32], such XRD diffractogram is attributed to a fully ordered cubic $L2_1$ austenitic structure. Nevertheless, these two superlattices' diffraction (111) and (200) peaks are significantly weaker as compared to other superlattices' peaks belonging to the same diffractogram. Therefore, the intensities of these peaks may be essentially undetectable if the majority or all of the elements in the present alloys belong to the same period in the elemental periodic table [37]. Commonly, these two XRD diffraction lines will not appear if samples demonstrate such a disordered cubic A2 crystal structure [38]. Given that Mn ($3d^5 4s^2$) and Co ($3d^7 4s^2$) belong to the same period (period 4) in the periodic table, GCMW-B, i.e., $\rho = 0.42$, may have a disordered phase with the cubic A2 type structure. Moreover, in this diffractogram, we can observe the absence of a (400) peak around $2\Theta = 65°$, the presence of which is usually expected in the A2 structure. There is a possibility that the crystallites are too fine to be recognized via X-rays, as previously noticed [39]. For the $2\Theta < 25°$, GCMW-A and GCMW-B have a noticeable halo originating from the glass coating layers, as reported in our previous works [19,30–32]. Another XRD analysis is obtained for the samples with $\rho = 0.46$, where mixed structures with $L2_1$ and B2 embedded with the amorphous halo are observed. The order and disordered microstructure overlap with the amorphous halo in this sample. For a more detailed explanation, see [29]. Additionally, similar scattering effects of the constituent elements (Co, Mn, and Si) can explain the absence of some XRD peaks [40]. Subsequently, when both XRD spectra are compared, the well-defined diffraction patterns presented in GCMW-A reflect high crystallinity. The intensity of the diffraction peak then weakens with increasing the ρ-ratio, as reported and discussed in our previous investigations [41]. This proves that with relatively low crystallinity, the crystalline size diminishes compared to GCMWs-B. It is important to note that superstructure peak intensities can be affected by various types of atomic disorder [19]. As we know, Co_2MnSi compounds can be described as X_2YZ Heusler alloy types. Therefore, for a deeper understanding of the $L2_1$ and A2 phases, the arrangement of atoms in both crystal structures can be discussed. It can be realized that the $L2_1$-type belongs to the cubic $Fm\overline{3}m$ space group, which is made up of four interpenetrated face-centered cubic (FCC) sublattices. Considering the X_2YZ type, in our case, Co (X), Mn (Y), and Si (Z) occupy the following Wyckoff positions: Si (Z) is the main group element with the highest electronegativity, which occupies 4a (0 0 0), Mn (Y) is the lower-valence transition metal atom with the smallest electronegativity, occupies 4b (0.5 0.5 0.5), and Co, the transition metal (X) atoms, are of intermediate electronegativity and occupy 8c (0.25 0.25 0.25) and (0.75 0.75 0.75) [42].

Theoretically, under 2θ ranging, (220) and (400) are the main reflection peaks of the $L2_1$ structure, although (111) and (200) sublattices are responsible for the orderly stacking of X, Y, and Z atoms. Heusler alloys with an ordered cubic $L2_1$ structure are specifically identified by the existence of super lattice reflection peaks; the presence of the (111) peak indicates the chemical ordering of atoms in octahedral positions, the (200) peak implies the order for atoms in tetrahedral positions, and the (220) peak is a principal reflection that is independent of the state of the order. Therefore, the diffractogram of GCMW-B confirms the disordered A2-type cubic structure with no ordered reflection. A random distribution of atoms over lattice sites ultimately leads to the formation of an A2 (bcc) disorder structure [43].

Crystallographic parameters, such as the space group, cell parameters, crystallite size, and Strukturbericht designation of two cubic phases of GCMW-A, GCMW-B, and GCMWs** are provided in Table 2.
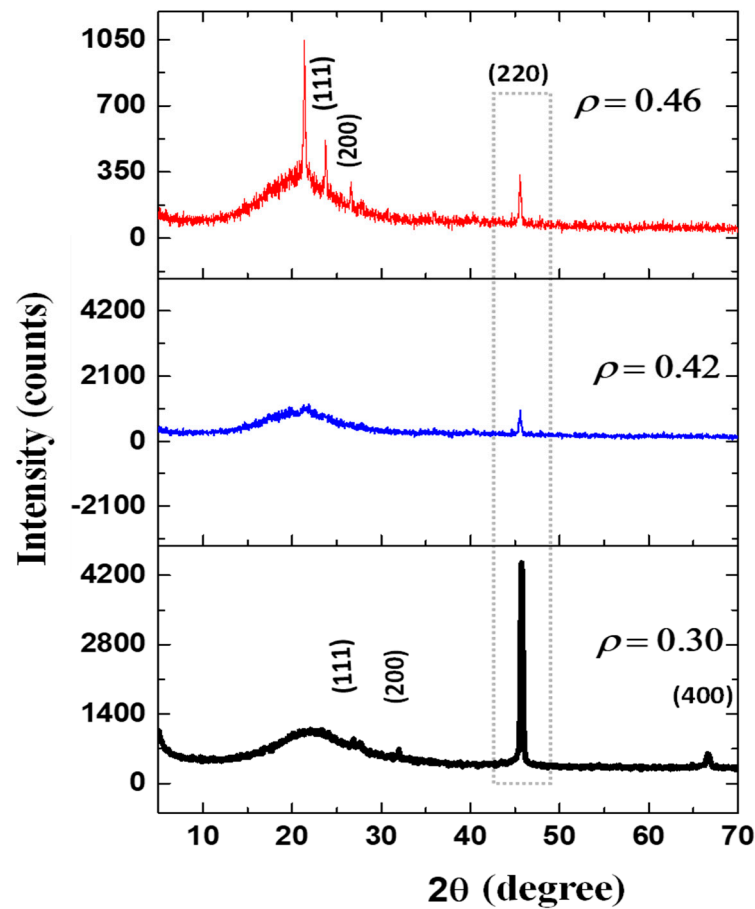
Figure 2. Room temperature X-ray diffraction (XRD) diffractograms of Co_2MnSi for GCMWs-A, GCMWs-B, and GCMWs**.

Table 2. Crystallographic information of prepared Co_2MnSi glass-coated microwires (GCMW-A, GCMW-B, and GCMWs**).

Sample	Crystallite Size (nm)	Space Group	Cell Parameters	Strukturbericht Designation
GCMWs-A	37 ± 0.1	$Fm3\overline{\ }m$ (FCC)	$a = 5.62 \text{ A}^0$	$L2_1$
GCMWs-B	28 ± 0.1	$Im3\overline{\ }m$ (BCC)	$a = 2.87 \text{ A}^0$	A2
GCMWs**	46 ± 0.1	$Fm3\overline{\ }m$ (FCC)	$a = 5.62 \text{ A}^0$	$L2_1$&B2

GCMWs**: Co_2MnSi glass-coated microwires with ($\rho = 0.46$) [29].

3.2. Magnetic Properties (M-H Behavior)

The magnetic properties of Co_2MnSi glass-coated microwires are linked to their structure. The combination of a metallic nucleus and a glass coating affects the magnetic properties. To study the magnetic properties of the samples, magnetization measurements were carried out. For better comparison of the M-H loops of both GCMWs, the magnetic hysteresis (M-H) loops are normalized and expressed as M/M_{5K}, where M_{5K} is the maximal magnetic moment attained at 5 K (lower temperature). Figure 3 shows the evolution of hysteresis loops of Co_2MnSi glass-coated microwires over the temperature range from 5 K to 300 K. As illustrated in Figure 3, all samples with different ρ-ratios exhibit ferromagnetic behavior.

Generally, coercivity (Hc) is an essential parameter in magnetic material characterization, as it determines their practical utility for specific applications. The coercivity of ferromagnetic glass-coated microwires can vary depending on several factors, including

the composition of the metallic nucleus, the dimensions of the microwire, and the manufacturing process conditions. It is important to note that the choice of ferromagnetic material, in combination with the microwire dimensions and the specific application requirements, determines the coercivity of glass-coated microwires. Therefore, the coercivity can be tailored by selecting appropriate core materials and optimizing the fabrication process of the microwires [33,44,45]. Table 3 summarizes the Hc values of GCMW-A, GCMW-B, and GCMWs for a wide range of temperatures from 5 to 300 K. For GCMW-A, the coercivity values vary between 8.5 and 11.2 Oe. However, Hc values fluctuate between 5.3 and 9.2 Oe for GCMW-B and GCMWs, respectively. The differences between the highest and lowest values of coercivity can indicate the temperature stability of Hc. Thus, the GCMWs-A sample shows higher thermal stability compared to the GCMW-B sample, where ΔHc = 2.7 Oe for the B sample and 3.9 Oe for the GCMW-B and GCMWs samples, respectively.
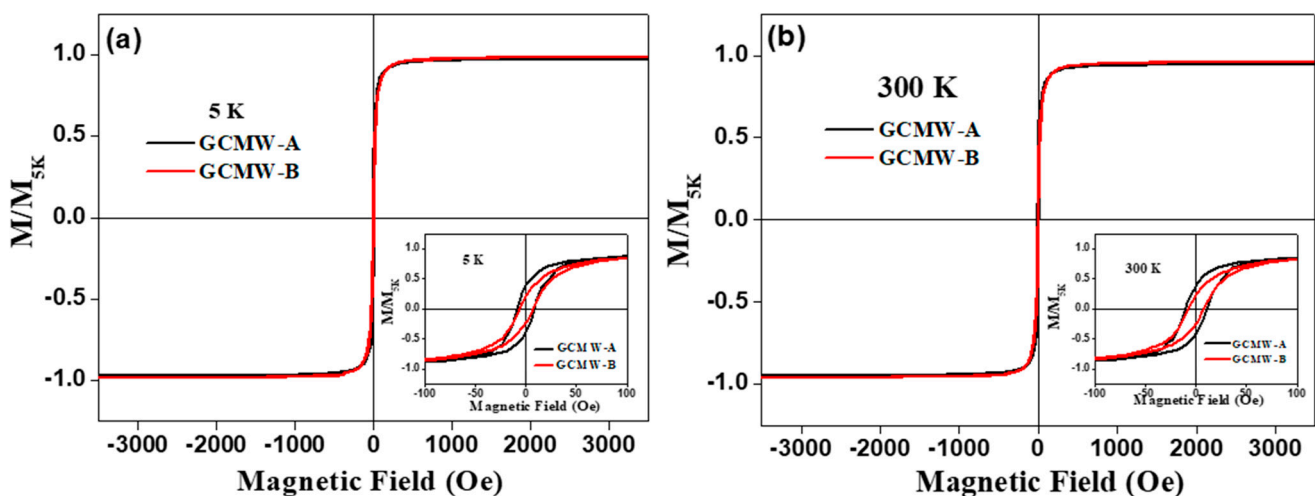

Figure 3. Hysteresis loops measured at (**a**) 5 K and (**b**) 300 K for Co_2MnSi GCMW-A and GCMW-B. (The insets show (**a**,**b**) the low-scale M-H loops of samples).

Table 3. Coercivity dependence on temperature of prepared Co_2MnSi glass-coated microwires (GCMW-A and GCMW-B).

T(K)	GCMW-A	GCMW-B	P Factor
	H_c (Oe)	H_c (Oe)	H_c (A)/H_c (B)
5	11.2 $\pm$ 0.5	7.2 $\pm$ 0.5	1.6
20	9.7 $\pm$ 0.5	5.3 $\pm$ 0.5	1.8
50	9.6 $\pm$ 0.5	7.1 $\pm$ 0.5	1.4
100	9.7 $\pm$ 0.5	6.8 $\pm$ 0.5	1.4
150	8.5 $\pm$ 0.5	6.5 $\pm$ 0.5	1.3
200	9.7 $\pm$ 0.5	8.2 $\pm$ 0.5	1.2
250	9.1 $\pm$ 0.5	8.4 $\pm$ 0.5	1.1
300	10 $\pm$ 0.5	9.2 $\pm$ 0.5	1.1
ΔHc	2.7	3.9	

Considering this thermal stability factor, i.e., P = Hc (A)/Hc (B), P > 1 indicates that GCMWs-A show a higher Hc value as compared to GCMW-B. As shown in Table 3, the P factor shows a monotonic increase with temperature, and by decreasing the temperature from 300 to 20 K, the P increases from 1.1 to 1.8 at T = 20 K. A decrease in the P-factor from 1.8 to 1.6 is observed below T = 20 K and is related to strong changes in the magnetic behavior of GCMW-A and GCMW-B at low temperatures. The observed results and

behavior of Hc and P with T (K) indicate a strong dependence of the magnetic properties on the aspect ratio.

3.3. Magnetic Properties (ZFC, FC, and FH Magnetization Behavior)

To investigate the impact of the microstructure ordering on the magnetothermal behavior of Co_2MnSi-GCMWs samples, zero field cooling (ZFC), field cooling (FC), and field heating (FH) magnetization measurements have been performed at different temperatures and magnetic fields. All magnetic curves are normalized to M/M_{5K} for a better comparison of the studied samples.

When a weak external magnetic field is applied, i.e., H = 50 Oe, noticeable differences are observed when measuring the ZFC, FC, and FH curves for the ordered sample (GCMW-A) and the disordered sample (GCMW-B) (see Figure 4). Both samples show large irreversibility: the magnetization curves start to decrease by decreasing the temperature from 350 K to 5 K. The characteristic point, such as the irreversible temperature (Tirr) for the ordered sample, has shifted to the low temperature (Tirr ≥ 120 K); however, Tirr ≈ 175 K for the disordered sample. The ZFC, FC, and FH curves appear to match perfectly in a temperature range from 350 K to 70 K, while below T = 70 Ka, a notable mismatch between the FC and ZFC is detected. For the ordered sample, a notable mismatch between the ZFC, FC, and FH curves is observed (see Figure 4a). Assuming the difference between magnetization curves as (ΔM), ΔM between ZFC and FC&FH is much higher than ΔM between FH and FC for the ordered sample at all measuring temperatures. In contrast, ΔM ≈ 0 for the disordered sample at a temperature range of 350–70 K.

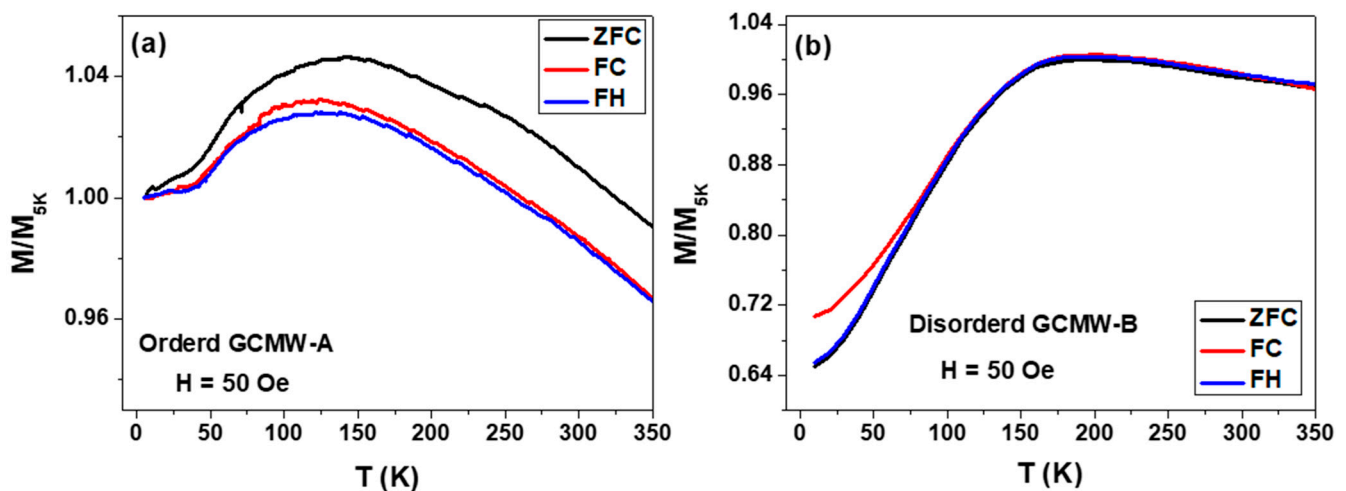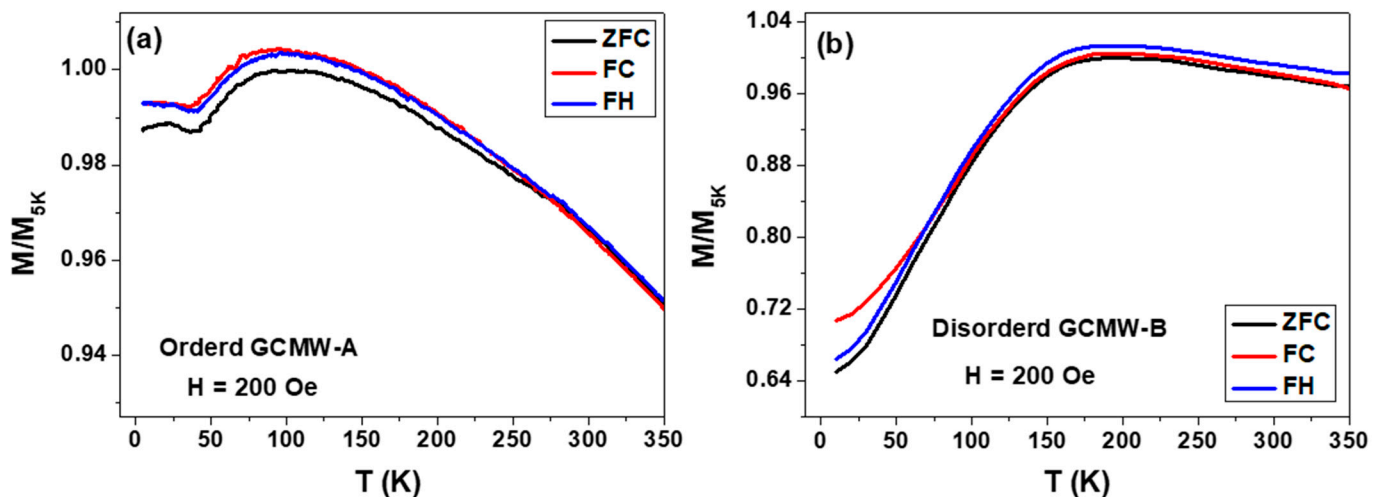**Figure 4.** Temperature dependence of magnetization M/M_{5K} (H) for prepared Co_2MnSi glass-coated microwires A (**a**) and B (**b**) with applied external magnetic field of 50 Oe.

Upon further increasing the external magnetic field from 50 Oe to 200 Oe, a slight change in the magnetic behavior of the disordered sample is observed, where ΔM between ZFC and FC&FH increases slightly. However, for the ordered sample, ΔM for ZFC, FC, and FH curves is almost zero at temperatures ranging from 350 to 260 K (see Figure 5a). In addition, the FC and FH curves overlap the ZFC curves for temperatures below 260 K. Moreover, an additional transition point appears at T = 35 K, where the behavior of ZFC, FC, and FH curves starts changing and increases with decreasing temperature from 35 to 5 K.

Increasing the external magnetic field up to 1 kOe while measuring the ZFC, FC, and FH magnetic curves has a strong effect on the magnetic behavior of the disordered sample. In the ordered sample (GCMW-A), the ZFC, FC, and FH curves show perfect matching with two flipping points at T = 85 K and T = 45 K, where the magnetic behavior changed, as described in Figure 6a. Meanwhile, the disordered sample shows inhomogeneous magnetic behavior, where ZFC, FC, and FH do not match. In addition, there is a notable

characteristic temperature at which the magnetic behavior changes. As illustrated in Figure 6b, for disordered samples, the magnetic behavior of ZFC, FC, and FH can be divided into two main parts depending on the temperature range. The first part is observed for the temperature range 350–225 K, where FC and FH monotonically increase as the temperature decreases until reaching a maximum value at T = 225 K. Then, below this temperature, a decrease in the FC and FH curves is observed with a further decrease in temperature until a minimum is reached at 5 K (see Figure 6b). The most interesting point is that the thermal magnetic behavior of the disordered sample shows a trend opposite to that of the ordered one when the applied field changes from 50 Oe to 1000 Oe.

Figure 5. Temperature dependence of magnetization M/M_{5K} (H) for prepared Co_2MnSi glass-coated microwires A (**a**) and B (**b**) with applied external magnetic field of 200 Oe.
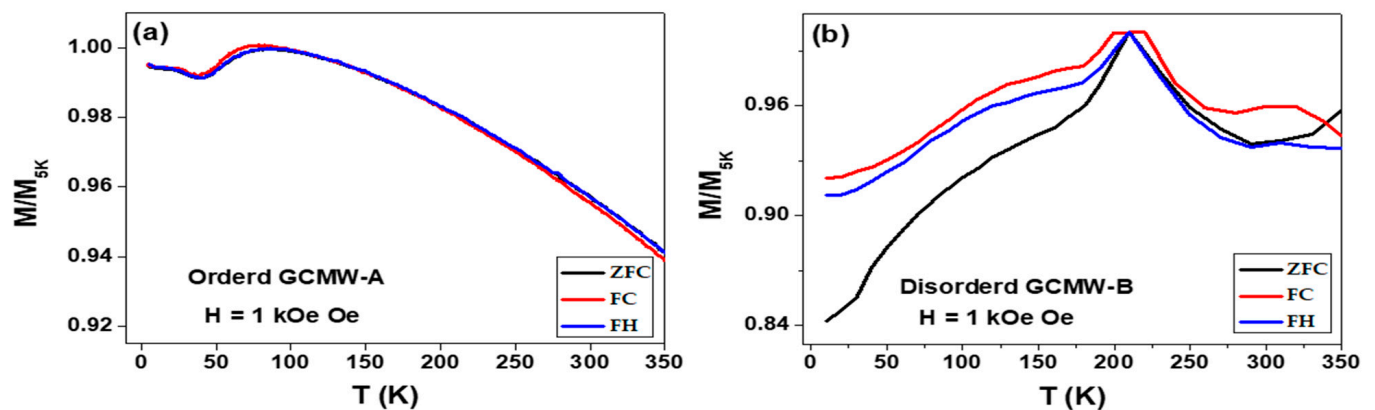

Figure 6. Temperature dependence of magnetization M/M_{5K} (H) for synthesized Co_2MnSi glass-coated microwires A (**a**) and B (**b**) with applied external magnetic field of 1 kOe.

4. Discussion

The Taylor–Ulitovsky manufacturing process involves various parameters that can affect the metallic nucleus diameter and glass coating thickness of the produced glass-coated microwires. Among these factors are the speed at which the wire is drawn, the glass tube feed, or the ingot temperature [22]. There are several sources of internal stresses, such as the difference in the thermal expansion coefficients of metallic alloy solidifying inside the glass coating, the quenching stresses related to the rapid quenching of the metallic alloy, and the drawing stresses [22,26,36]. The stresses induced by the difference in the thermal expansion coefficients of metallic alloy and the glass coating are the largest, being an order of magnitude higher than the other stresses [22,36]. The thicker the glass coating, the

stronger the internal stresses. Accordingly, the internal stresses can be modified using the ratio of the metallic nucleus to the entire diameter. Thus, raising the d/D ratio diminishes the stresses caused by the shell [22,26,36]. However, it must be taken into account that the quenching rate of the metallic alloy is affected by the thickness of the insulating glass coating [22]. Therefore, the crystalline structure can be also affected by the glass-coating thickness [22,46,47]. Additionally, the influence of the internal stresses on the crystallization process must be related to the non-equilibrium thermodynamics: the crystal's nucleation and growth are affected by the atomic diffusion in the presence of the stress [48]. From studies of Co_2MnSi microwires, we can deduce that decreasing the d/D ratio from 0.42 (GCMW-B) to 0.30 (GCMW-A) can lead to enhancing the crystallinity and the degree of structural order from a disordered A2 type to an ordered $L2_1$ cubic structure. Furthermore, changing the geometrical parameters has a huge effect on magnetic behavior. When compared to GCMW-B and GCMWs**, the magnetic behavior of GCMW-A can be significantly modified by applying a moderate magnetic field of 200 Oe instead of 50 Oe. This can be explained by the sensitivity of GCMW-A to small magnetic field changes. However, substantial variations in the magnetic behavior of GCMW-B by applying 1 kOe are detected. Thus, such modification in GCMW-B and GCMWs** magnetic behavior is correlated with the X-ray diffraction results, owing to the disordered A2 cubic structure. Moreover, the magnetization curves in GCMW-A tend to overlap gradually by increasing the magnetic field application from 50 Oe to 1 kOe. Therefore, glass-coated Co_2MnSi microwires are sensitive to changing temperature and applied magnetic field, as demonstrated by the magnetic behavior of the GCMW-A sample, making them an appropriate candidate for use as sensing materials.

The obtained results illustrate the strong dependence of the microstructure and thermomagnetic properties of rather well-known Heusler alloys, i.e., Co_2MnSi-based glass coating microwires on its geometric parameters. The ability to tailor the magnetic and structure properties of Heusler-based glass-coated microwires makes these smart systems promising for different applications.

5. Conclusions

In this study, we illustrate the effect of changing geometrical parameters during the manufacturing process of Co_2MnSi glass-coated microwires on the structure and magnetic properties. Two Co_2MnSi microwires coated with glass are produced employing the Taylor–Utilovsky method by changing the metallic nucleus and total diameters of the microwire. From the X-ray analysis, we observed that GCMW-A exhibits an $L2_1$ cubic ordered structure with the $Fm\overline{3}m$ space group, whereas GCMW-B demonstrates an A2 cubic disordered structure with the $Im\overline{3}m$ space group. By comparing both XRD diffractograms, the well-defined diffraction peaks presented in GCMW-A indicate their high crystallinity. Thus, the intensity of the diffraction peak decreases with increasing aspect ratio. This proves that, with relatively low crystallinity, the crystalline size diminishes from 37 to 28.02 nm with an increasing aspect ratio. In terms of magnetic properties, both samples display different magnetic responses to temperature and applied magnetic field. First, when a field of 50 Oe is applied, the ZFC-FC-FH magnetization curves exhibit irreversible magnetic behavior, accompanied by a mismatch between the ZFC and FH curves. Furthermore, when a magnetic field of 200 Oe is applied, no changes were observed in the (M, T) curves of GCMW-B. However, applying a magnetic field of 200 Oe to GCMW-A reduces the difference between the ZFC and FH magnetization curves. When a stronger magnetic field of 1 kOe is applied, the ZFC and FH magnetization curves in GCMW-A coincide, but GCMW-B exhibits a strong change and mismatch related to the disordered crystalline structure. Because of the extraordinary thermal stability of the coercivity values of GCMW-A, GCMW-B, and GCMWs**, Co_2MnSi microwires can be used in generator, sensor, transformer, and actuator applications.

References

1. Manna, K.; Sun, Y.; Muechler, L.; Kübler, J.; Felser, C. Heusler, weyl and berry. *Nat. Rev. Mater.* **2018**, *3*, 244–256. [CrossRef]
2. Sheron, T.; Kesong, Y.; Marc, A.M. Heusler alloys: Past, properties, new alloys, and prospects. *Prog. Mater. Sci.* **2023**, *132*, 101017. [CrossRef]
3. Balke, B.; Wurmehl, S.; Fecher, G.H.; Felser, C.; Kübler, K. Rational design of new materials for spintronics: Co_2FeZ (Z=Al, Ga, Si, Ge). *Sci. Technol. Adv. Mater.* **2008**, *9*, 1. [CrossRef] [PubMed]
4. Galanakis, I. Theory of Heusler and Full-Heusler Compounds. In *Heusler Alloys*; Felser, C., Hirohata, A., Eds.; Springer Series in Materials Science; Springer: Cham, Switzerland, 2016; Volume 222. [CrossRef]
5. Trudel, S.; Gaier, O.; Hamrle, J.; Hillebrands, B. Magnetic Anisotropy, Exchange and Damping in Cobalt-Based Full-Heusler Compounds: An Experimental Review. *J. Phys. D. Appl. Phys.* **2010**, *43*, 193001. [CrossRef]
6. Graf, T.; Felser, C.; Parkin, S.S.P. Simple Rules for the Understanding of Heusler Compounds. *Prog. Solid. State Chem.* **2011**, *39*, 1–50. [CrossRef]
7. Adem, U.; Dincer, I.; Aktürk, S.; Acet, M.; Elerman, Y. Phase Formation Characteristics and Magnetic Properties of Bulk Ni2MnGe Heusler Alloy. *J. Alloys Compd.* **2015**, *618*, 115–119. [CrossRef]
8. Hazra, B.K.; Kaul, S.N.; Srinath, S.; Raja, M.M. Uniaxial Anisotropy, Intrinsic and Extrinsic Damping in Co_2FeSi Heusler Alloy Thin Films. *J. Phys. D. Appl. Phys.* **2019**, *52*, 325002. [CrossRef]
9. Yu, L.; Li, Z.; Zhu, J.; Liu, H.; Zhang, Y.; Cao, Y.; Xu, K.; Liu, Y. Electrical and Magnetic Transport Properties of Co_2VGa Half-Metallic Heusler Alloy. *Materials* **2022**, *15*, 6138. [CrossRef]
10. Bentouaf, A.; Hassan, F.H.; Reshak, A.H.; Aïssa, B.; Aïssa, A. First-Principles Study on the Structural, Electronic, Magnetic and Thermodynamic Properties of Full Heusler Alloys Co_2VZ (Z = Al, Ga). *J. Electron. Mater.* **2017**, *46*, 130–142. [CrossRef]
11. Dong, Z.; Luo, J.; Wang, C.; Jiang, Y.; Tan, S.; Zhang, Y.; Grin, Y.; Yu, Z.; Guo, K.; Zhang, J.; et al. Half-Heusler-like compounds with wide continuous compositions and tunable p- to n-type semiconducting thermoelectrics. *Nat. Commun.* **2022**, *13*, 35. [CrossRef]
12. Enkatesan, A.; Govindan, S.; Kalaimani, K.R.; Kuppan, R. Impact of annealing temperature on structural and magnetic properties of Co_2FeSn Heusler alloy. *J. Magn. Magn. Mater.* **2020**, *508*, 166731. [CrossRef]
13. Matyja, E.; Prusik, K.; Zubko, M.; Świec, P.; Dercz, G.; Loskot, J. Crystallization Kinetics and Structure Evolution during Annealing of Ni-Co-Mn-In Powders Obtained by Mechanical Alloying. *Materials* **2023**, *16*, 645. [CrossRef]
14. Ahmed, S.J.; Boyer, C.; Niewczas, M. Magnetic and structural properties of Co_2MnSi based Heusler compound. *J. Alloys Compd.* **2018**, *12*, 018. [CrossRef]
15. Wederni, A.; Ipatov, M.; Pineda, E.; Suñol, J.-J.; Escoda, L.; González, J.M.; Alleg, S.; Khitouni, M.; Żuberek, R.; Chumak, O.; et al. Magnetic Properties, Martensitic and Magnetostructural Transformations of Ferromagnetic Ni–Mn–Sn–Cu Shape Memory Alloys. *Appl. Phys.* **2020**, *126*, 320. [CrossRef]
16. Wederni, A.; Ipatov, M.; González, J.M.; Khitouni, M.; Suñol, J.J. Ni-Mn-Sn-Cu Alloys after Thermal Cycling: Thermal and Magnetic Response. *Materials* **2021**, *14*, 6851. [CrossRef] [PubMed]
17. Wederni, A.; Ipatov, M.; Pineda, E.; Escoda, L.; González, J.-M.; Khitouni, M.; Suñol, J.-J. Martensitic Transformation, Thermal Analysis and Magnetocaloric Properties of Ni-Mn-Sn-Pd Alloys. *Processes* **2020**, *8*, 1582. [CrossRef]

18. Dhanal, S.V.; Devadi, H.; Akkimardi, V.G.; Kori, S.A. INDIAN JOURNAL OF SCIENCE AND TECHNOLOGY Ni-Mn-Al Heusler Alloy Samples Preparation by Mechanical Alloying Method and Study of Their Investigated Properties. *Prop. Indian J. Sci. Technol.* **2022**, *15*, 1997–2003. [CrossRef]

19. Salaheldeen, M.; Wederni, A.; Ipatov, M.; Zhukova, V.; Zhukov, A. Preparation and Magneto-Structural Investigation of High Ordered (L2_1 Structure) Co$_2$MnGe Microwires. *Processes* **2023**, *11*, 1138. [CrossRef]

20. Liu, S.; Cao, P.; Lin, D.Y.; Tian, F. Stability of L21 (NiM)$_2$TiAl (M=Co, Fe) in High-Entropy Alloys. *J. Alloys Compd.* **2018**, *764*, 650–655. [CrossRef]

21. Sofi, S.A.; Gupta, D.C. Exploration of Electronic Structure, Mechanical Stability, Magnetism, and Thermophysical Properties of L21 Structured Co$_2$XSb (X = Sc and Ti) Ferromagnets. *Int. J. Energy Res.* **2020**, *44*, 2137–2149. [CrossRef]

22. Zhukov, A.; Corte-Leon, P.; Gonzalez-Legarreta, L.; Ipatov, M.; Blanco, J.M.; Gonzalez, A.; Zhukova, V. Advanced Functional Magnetic Microwires for Technological Applications. *J. Phys. D Appl. Phys.* **2022**, *55*, 253003. [CrossRef]

23. Ulitovsky, A.V.; Maianski, I.M.; Avramenco, A.I. 1960 Method of Continuous Casting of Glass Coated Microwire. USSR Patent 128427, 6 May 2015. Bulletin, No 10, p. 14.

24. Salaheldeen, M.; Wederni, A.; Ipatov, M.; Zhukova, V.; Zhukov, A. Carbon-Doped Co$_2$MnSi Heusler Alloy Microwires with Improved Thermal Characteristics of Magnetization for Multifunctional Applications. *Materials* **2023**, *16*, 5333. [CrossRef] [PubMed]

25. Hennel, M.; Galdun, L.; Varga, R. Analysis of magnetocaloric effect in Ni$_2$FeGa-based glass-coated microwire. *J. Magn. Magn. Mater.* **2022**, *560*, 169646. [CrossRef]

26. Chiriac, H.; Ovari, T.-A. Amorphous glass-covered magnetic wires: Preparation, properties, applications. *Prog. Mater. Sci.* **1996**, *40*, 333–407. [CrossRef]

27. Baranov, S.A.; Larin, V.S.; Torcunov, A.V. Technology, Preparation and Properties of the Cast Glass-Coated Magnetic Microwires. *Crystals* **2017**, *7*, 136. [CrossRef]

28. Aronin, A.S.; Abrosimova, G.E.; Kiselev, A.P.; Zhukova, V.; Varga, R.; Zhukov, A. The effect of mechanical stress on Ni$_{63.8}$Mn$_{11.1}$Ga$_{25.1}$ microwire crystalline structure and properties. *Intermetallics* **2013**, *43*, 60–64. [CrossRef]

29. Salaheldeen, M.; Talaat, A.; Ipatov, M.; Zhukova, V.; Zhukov, A. Preparation and Magneto-Structural Investigation of Nanocrystalline CoMn-Based Heusler Alloy Glass-Coated Microwires. *Processes* **2022**, *10*, 2248. [CrossRef]

30. Salaheldeen, M.; Ipatov, M.; Corte-Leon, P.; Zhukova, V.; Zhukov, A. Effect of Annealing on the Magnetic Properties of Co$_2$MnSi-Based Heusler Alloy Glass-Coated Microwires. *Metals* **2023**, *13*, 412. [CrossRef]

31. Salaheldeen, M.; Zhukova, V.; Wederni, A.; Ipatov, M.; Zhukov, A. Magnetic Properties of Co$_2$MnSi-based Heusler Alloy Glass-coated Microwires. *IEEE Trans. Magn.* **2023**. [CrossRef]

32. Salaheldeen, M.; Wederni, A.; Ipatov, M.; Gonzalez, J.; Zhukova, V.; Zhukov, A. Elucidation of the Strong Effect of the Annealing and the Magnetic Field on the Magnetic Properties of Ni$_2$-Based Heusler Microwires. *Crystals* **2022**, *12*, 1755. [CrossRef]

33. Cobeño, A.F.; Zhukov, A.; de Arellano-Lopez, A.R.; Elías, F.; Blanco, J.M.; Larin, V.; González, J. Physical properties of nearly zero magnetostriction Co-rich glass-coated amorphous microwires. *J. Mater. Res.* **1999**, *14*, 3775–3783. [CrossRef]

34. Nematov, M.G.; Baraban, I.; Yudanov, N.A.; Rodionova, V.; Qin, F.X.; Peng, H.X.; Panina, L.V. Evolution of the magnetic anisotropy and magnetostriction in Co-based amorphous alloys microwires due to current annealing and stress-sensory applications. *J. Alloys Compd.* **2020**, *837*, 155584. [CrossRef]

35. Fuks, A.; Abrosimova, G.; Aksenov, O.; Churyukanova, M.; Aronin, A. The Influence of Internal Stress on the Nanocrystal Formation of Amorphous Fe$_{73.8}$Si$_{13}$B$_{9.1}$Cu$_1$Nb$_{3.1}$ Microwires and Ribbons. *Crystals* **2022**, *12*, 1494. [CrossRef]

36. Astefanoaei, I.; Radu, D.; Chiriac, H. Internal stress distribution in DC joule-heated amorphous glass-covered microwires. *J. Phys. Condens. Matter.* **2006**, *18*, 2689–2716. [CrossRef]

37. Salaheldeen, M.; Garcia, A.; Corte-Leon, P.; Ipatov, M.; Zhukova, V.; Zhukov, A. Unveiling the Effect of Annealing on Magnetic Properties of Nanocrystalline Half-Metallic Heusler Co$_2$FeSi Alloy Glass-Coated Microwires. *J. Mater. Res. Technol.* **2022**, *20*, 4161–4172. [CrossRef]

38. Elphick, K.; Frost, W.; Samiepour, M.; Kubota, T.; Takanashi, K.; Sukegawa, H.; Mitani, S.; Hirohata, A. Heusler Alloys for Spintronic Devices: Review on Recent Development and Future Perspectives. *Sci. Technol. Adv. Mate.* **2021**, *22*, 235–271. [CrossRef]

39. Wang, K.; Xu, Z.; Fu, X.; Lu, Z.; Xiong, R. Magnetic and Structural Properties of Sputtered Thick Co$_2$FeSi Alloy Films. *J. Magn. Magn. Mater.* **2023**, *570*, 170557. [CrossRef]

40. Zhang, X.; Han, L.; Dehm, G.; Liebscher, C.H. Microstructure and Physical Properties of Dual-Phase Soft Magnetic Fe-Co-Ti-Ge Alloys. *J. Alloys Compd.* **2023**, *945*, 169282. [CrossRef]

41. Salaheldeen, M.; Wederni, A.; Ipatov, M.; Zhukova, V.; Lopez Anton, R.; Zhukov, A. Enhancing the Squareness and Bi-Phase Magnetic Switching of Co$_2$FeSi Microwires for Sensing Application. *Sensors* **2023**, *23*, 5109. [CrossRef]

42. Zhang, Y.; He, X.; Xu, K.; Kang, Y.; Sun, H.; Liu, H.; Cao, Y.; Wei, S.; Li, Z.; Jing, C. Structural Ordering, Magnetic and Electrical Transport Properties in Ni6$_{0-X}$Fe$_{13+x}$Ga$_{27}$ Heusler Alloys. *J. Alloys Compd.* **2023**, *936*, 168242. [CrossRef]

43. Mahat, R.; Karki, U.; Shambhu, K.C.; Law, J.Y.; Franco, V.; Galanakis, I.; Gupta, A.; Leclair, P. Effect of Mixing the Low-Valence Transition Metal Atoms Y = Co, Fe, Mn, Cr, V, Ti, or Sc on the Properties of Quaternary Heusler Compounds Co$_{2-x}$Y$_x$FeSi ($0 \leq x \leq 1$). *Phys. Rev. Mater.* **2022**, *6*, 064413. [CrossRef]

44. Salaheldeen, M.; Garcia-Gomez, A.; Ipatov, M.; Corte-Leon, P.; Zhukova, V.; Blanco, J.M.; Zhukov, A. Fabrication and Magneto-Structural Properties of Co_2-Based Heusler Alloy Glass-Coated Microwires with High Curie Temperature. *Chemosensors* **2022**, *10*, 225. [CrossRef]

45. Zhukova, V.; Cobeño, A.F.; Zhukov, A.; Blanco, J.M.; Larin, V.; Gonzalez, J. Coercivity of glass-coated $Fe_{73.4-x}Cu_1Nb_{3.1}Si_{13.4+x}B_{9.1}$ ($0 \leq x \leq 1.6$) microwires. *Nanostruct. Mater.* **1999**, *11*, 1319–1327. [CrossRef]

46. Salaheldeen, M.; Garcia-Gomez, A.; Corte-León, P.; Gonzalez, A.; Ipatov, M.; Zhukova, V.; Gonzalez, J.M.; López Antón, R.; Zhukov, A. Manipulation of Magnetic and Structure Properties of Ni_2FeSi Glass-Coated Microwires by Annealing. *J. Alloys Compd.* **2023**, *942*, 169026. [CrossRef]

47. Zhukov, A.; González, J.; Blanco, J.M.; Vázquez, M.; Larin, V. Microwires Coated by Glass: A New Family of Soft and Hard Magnetic Materials. *J. Mater. Res.* **2000**, *15*, 2107–2113. [CrossRef]

48. Onsager, L. Reciprocal Relations in Irreversible Processes. I. *Phys. Rev.* **1931**, *37*, 405. [CrossRef]